

3D Simulation of Packed Particle Bed and Transport Properties Prediction for Product Optimization through Virtual Experiments

*Supriyo Ghosh, N.C. State University, Raleigh, NC, Bruker Optics, The Woodlands, TX
Kevin M. Keener, Purdue University, West Lafayette, IN
Yong Pan, Procter & Gamble Co., Cincinnati, OH*

Abstract

Porous media are heterogeneous systems. The microstructures of the pore spaces influence their transport properties. A quantitative geometrical characterization of the pore space is crucial for accurate prediction of porous media transport. Thus, a 3D simulation of porous media was developed based on randomly packed glass beads. Unconsolidated porous media are reconstructed through Monte Carlo gravitational particle packing simulation. A mathematical morphology based three-dimensional image processing algorithm is developed to characterize the pore space in the simulated porous media. This algorithm calculates the bulk porosity, average particle contact numbers, and specific surface area of the porous media. It also generates the pore-throat network with details of pore size distribution, location, and throat tortuosity distribution. The simulation results are validated by statistical comparison with the bulk porosity and pore size distribution obtained from x-ray micro-tomographic images of randomly packed glass beads. Simulation of porous media, given a specific size distribution of constituent particles, followed by pore-space characterization provides a powerful tool for predicting transport processes.

Introduction

Transport in porous media is encountered in numerous physical systems from water resources management to industrial processes of varying length scales. It is a complex phenomenon.¹ Many efforts have been made to develop continuum mechanics based models to describe porous media transport.² These mathematical models often tried to correlate the transport behavior of a specific porous medium with their bulk porosity.³ Sometimes, in these models, effective permeability of the porous medium is represented as a function of porosity as well as an average tortuosity, in order to match the experimental data.⁴ These descriptions of porous media flow are not purely mechanistic models, but based on semi-empirical relationships among capillary pressure, saturation level, and relative permeability, obtained through controlled experiments.⁵ These models do not account for the topography of the microstructure in the porous medium. But, the transport of fluids and solutes in porous media is a function of its geometry and topological characteristics. The microscale phenomena happening in the pore-scale level translates very well into the macro-scale behavior of a porous structure.⁶ Hence, pore-network based modeling of various properties of porous media is a powerful method to generate realistic prediction of macroscopic behavior. Early attempts at pore network modeling describe porous media transport based on capillary tubes.⁷ These models attempted to explain the permeability without accounting for the interconnectivity among the pore channels. More recently the concept of 2D and 3D networks to describe the pore-space topography has been introduced.^{8,9} 2D pore networks have limited application since most porous media involve 3D flow and hence the the connectivity between pores can not usually be adequately defined in 2D.¹⁰ The existing 3D network models in the literature are not realistic, those are generated based on certain assumptions regarding the pore and throat size distribution.⁸

Thus, there is a need to develop a realistic 3D pore network model, which shows more promise to a realistic prediction of porous media transport. Pore network models can be generated using indirect or direct methods. In indirect method, an equivalent network is produced based on distributions of major pore-space structures, pore body and pore throat, and their positional correlations.¹¹ In contrast, the direct method, extracts the pore-throat network from the pore space directly using 3D image. The direct method requires no assumption related to the topological positions or dimensions. In order to directly map the pore network, a 3D data representing the pore-space, with enough resolution, is essential. Many attempts have been made to generate this dataset using high resolution non-invasive three-dimensional imaging techniques like laser scanning confocal microscopy¹², x-ray microtomography¹³, etc. There are three major limitations of this approach. First, one is restricted to investigating only those porous media, of which one already has samples of. Thus, one can not use this approach for virtual product design. Second, the pore-space data set resolution is limited by the instrument capability that is used to acquire the 3D data. The third limitation is the contrast in the dataset. The edges of the pore-space, i.e. the grain boundary in the instrument-generated images will not be absolute. This sharpness of the edges will depend on how the sample material interferes with the instrument signal. The imperfection in obtaining the correct edges can introduce serious errors in the pore network extracted.¹⁴ All these limitations are avoided in this work by extracting the pore network from a digitally generated consolidated porous media through computer simulation and mathematical morphology based image processing.

A random packing of particles represents an unconsolidated porous media. Various methods have been used by different researchers to generate a random packing of particles. Some of them are: sequential addition¹⁵, ballistic drop with mechanical interaction calculation¹⁶, region growing¹⁷, and mechanical contraction¹⁸. Simple rules of sequential addition, where particles are added at random positions as long as they do not share spaces with each other, can generate random particle packs, but the packing tend to be fairly loose.¹⁹ The reason for this is while placing a new particle it stops moving as soon as it hits another and do not slide along other particles boundary, which is more realistic. Ballistic drop method of random particle packing simulation utilizes calculations of mechanical forces each time a falling particle encounters another on its path. Although this method follows the mechanics of the process realistically and very accurately, many detailed calculations in each step of the movement for a huge number of particles become extremely demanding on the computing power. Thus, this method of simulation tends to be much slower, and to generate a random packing with fairly large numbers of particles, a very high amount of computing time is required. Region growing method of random particle packing is used in simulating aggregated powder particles. It starts with one central particle and attaches particles of random size at random available locations. This method is not representative of randomly dropping particles into a container randomly to generate an unconsolidated porous media.¹⁷ The mechanical contraction method of random particle packing is motivated by simulation of amorphous packing and is based on the idea of density quenching a system, which undergoes no thermal fluctuations. Three-dimensional Monte Carlo simulation under gravity is a method of random particle packing, which closely resembles random gravitational dropping of particles and at the same time computationally less demanding. Hence this method was selected to generate the porous media model in this work.

Since, the porous media models are constructed through computer simulations, the resolution of the pore-space was limited only by the available memory (RAM) and processor

speed of the computer used. This model enabled perfect binarization of 3D pore-space images without any error from edge or boundary detection.

A 3D image processing algorithm was developed for this work to map the pore-throat network. Skeletonization of the 3D pore-space was the first step in mapping of the pore-throat network. This conversion of the 3D image into the pore-throat network has a wide variety of applications and has been an active area of research for many decades.²⁰ Many researchers have tried different sequential, parallel, as well as non-iterative thinning techniques towards the same goal; Hamilton-Jacobi²¹, local flux driven extraction²², three-dimensional template based exclusion rule²³, medial axis extraction²⁴, are to name a few. These algorithms, in spite of being effective in finding the skeleton in specific kind of structural features, fail to correct centerline in other types of shape features.^{25,26,27} Especially when the structure is as complex as pore-space it becomes very challenging to come up with a single algorithm that will converge to a perfect skeleton in an unsupervised manner. A morphological thinning algorithm is developed in this work which thins the pore-space with same flux vector from all directions while preserving the continuity. This algorithm also generated the bulk porosity, co-ordination number, specific surface area. Using the distance-transform principle; pore size distribution, and average tortuosity of the pore-space are also calculated in an automated manner by this algorithm. All these values directly calculated from the three-dimensional morphology of the pore-space are more realistic input parameters for pore network based modeling. Thus porous media based virtual product design, aiming at a specific transport behavior, becomes much faster and complete.

Methods

Reconstruction Simulation

The three-dimensional Monte Carlo simulation algorithm in this work tries to simulate simultaneous random dropping of spherical particles, of a specific size distribution, into a container. As these particles finally take up mutually most stable positions, we obtain an unconsolidated porous media. The algorithm is built upon some assumptions, which are consistent with this final goal: (a) the particles are spherical in shape, (b) particle radii belong to a user specified distribution, (c) particles are rigid, (d) the container walls are rigid, (e) particles cannot move against the gravity i.e. upwards during their random motion, (f) downward and sidewise movement vectors of the particles are random. The algorithm starts with assignment of the particle number, its radius distribution shape, mean and width. It also prompts the user to provide the dimension of the container. Initially all the particles are allotted their center positions uniformly distributed in the container inner space. No location is accepted if it does not obey the assumptions (c) and (d), and that particle is reassigned another permissible location. During each iteration of the simulation the particles are moved sidewise and downward. The movement direction and magnitude are obtained by a normally distributed random number generation between -1 and +1 (in case of z-direction movement between -1 and 0), followed by multiplication with a factor commensurate with the length-scale of the system. As each iteration is completed, the total potential energy of the particle system with respect to the bottom floor of the container is calculated and stored in an array. With progress of the iterations the particle assembly gradually settles down towards the bottom of the container in a random fashion. The total potential energy of the system drops faster during initial few iterations and then gradually the rate decreases. As the slope of this total potential time-course becomes very close to zero, the iteration stops, and the final location of the particle centers and corresponding radii are recorded in proper matrices. A flow diagram of the

algorithm is given in figure 1. An example of 'movement of particles' during a Monte Carlo packing simulation is shown in figure 2. The time-course of the corresponding normalized total potential energy of the system as the simulation progresses is given in figure 3. A three-dimensional matrix is created based on the particle location and radii information. In this matrix the voxels occupied by the particles are assigned 0, and its complement set is assigned 1. This matrix now represents the pore-space. By adding all the voxels belonging to the pore space followed by division with the total number of voxels in the container gives the bulk porosity of the reconstructed porous medium.

In order to validate the simulation algorithm, a packed bed of spherical glass beads was obtained and a three-dimensional image is acquired using x-ray microtomography. During this measurement, x-ray passed through the glass bead pack. The attenuation in intensity of the x-ray as it passes through glass and air are distinctly different. Utilizing this contrast in attenuation coefficient of the transmitted x-ray a map of the glass bead pack was obtained. The x-ray microtomography system obtained multiple x-ray "shadow" transmission images of the packed bed from different angular views, as it rotates on a high precision stage. From these shadow images, cross-sectional images of the glass bead pack are reconstructed by a modified Feldkamp cone-beam algorithm, finally creating a complete three-dimensional representation of the internal microstructure. This image data was segmented into pore space and grains based on intensity difference, and the bulk porosity was calculated. The glass beads from the same lot are spread over a light microscope with bottom light configuration, and two-dimensional images are acquired. Images were obtained for approximately 1000 beads. An example image is shown in figure 5. An algorithm was developed to automate the process of finding the beads in those images, calculating their radii, and storing them in a data array. This array was then used to determine the shape, mean, and width of the distribution of the bead sizes. The distribution obtained for 500 μ diameter beads were shown in figure 6. This algorithm was validated by manually measuring 200 beads under the same microscope. This distribution was used as one of the input parameters while running the Monte Carlo packing simulation in triplicate. The bulk porosity, and pore size distributions were then obtained from the simulated packing and x-ray microtomography data, and compared statistically.

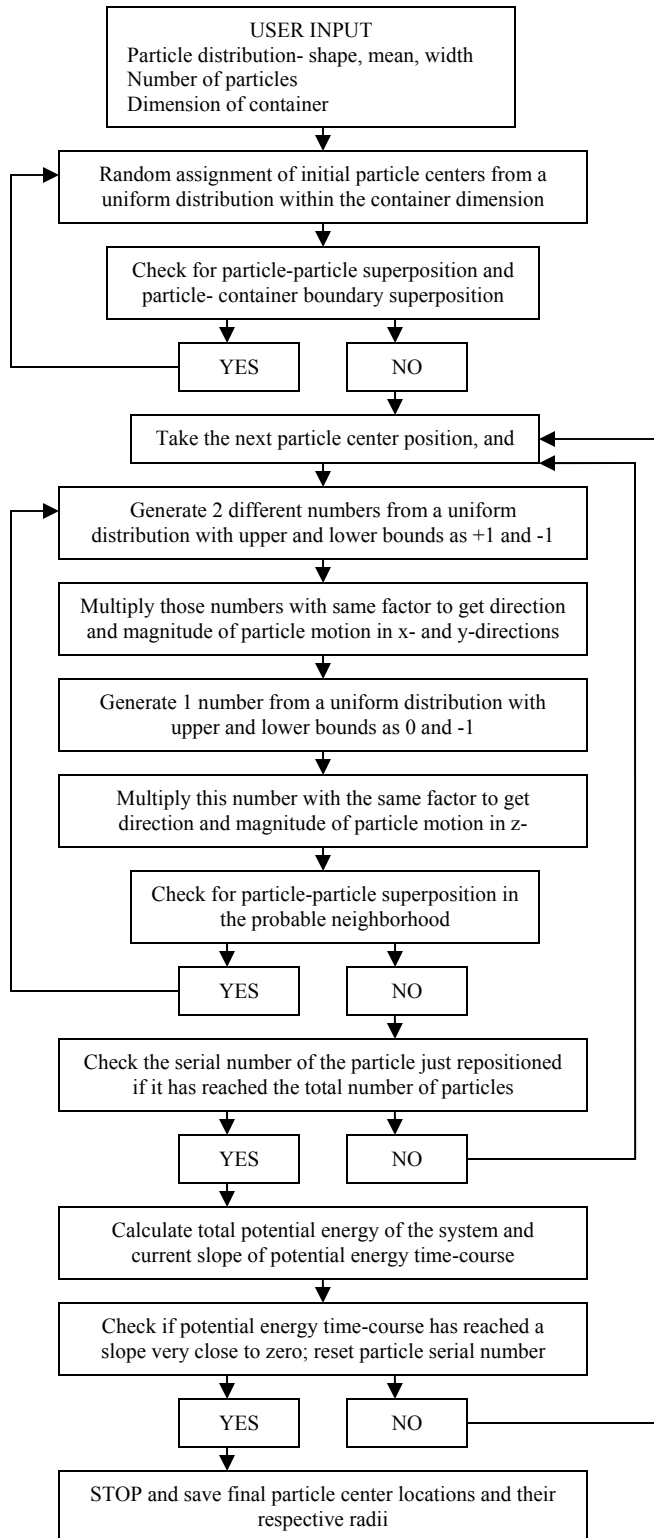


Figure 1: Monte Carlo gravitational particle packing simulation algorithm

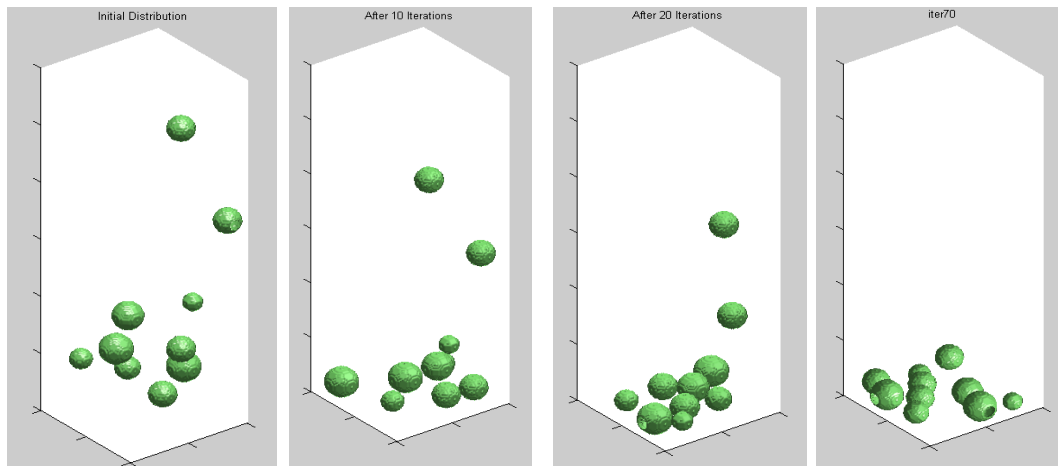


Figure 2: Example of movement of particles undergoing Monte Carlo gravitational simulation

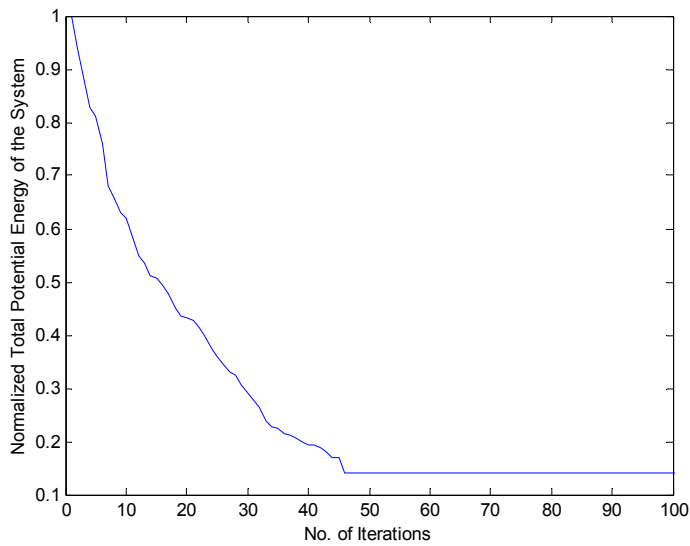


Figure 3: Normalized total potential energy of the particle system as the simulation progresses

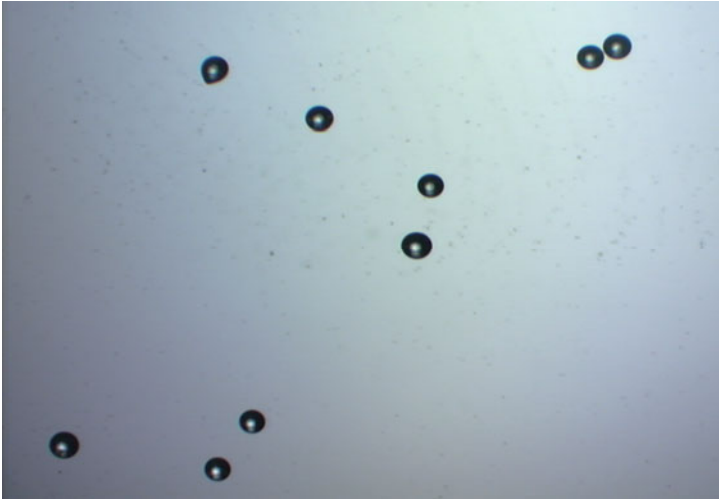


Figure 4: An example of acquired microscopic images of glass beads

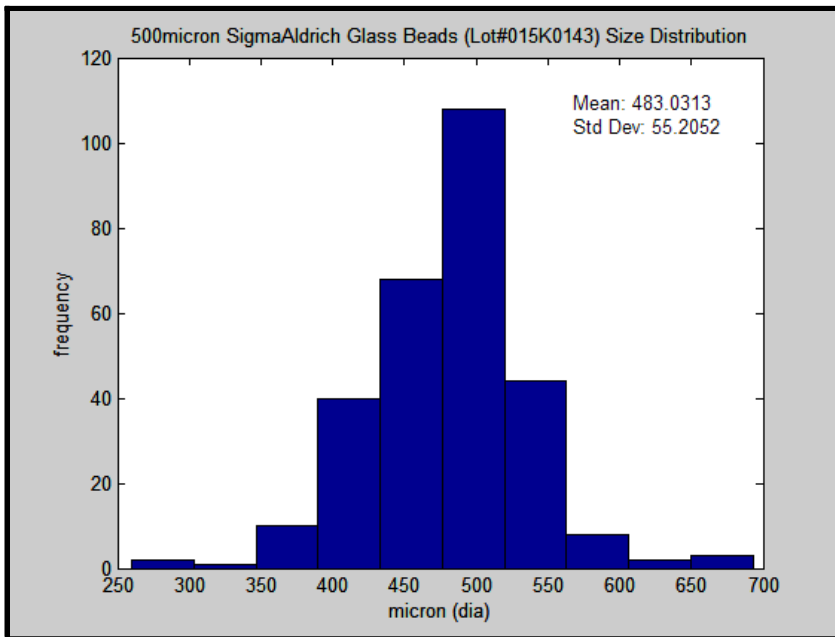


Figure 5: Distribution of glass bead sizes through automated microscopic image analysis

Image Processing

The image processing algorithm starts with the pore-space binarized three-dimensional data set. Each iteration in the algorithm executes the following set of actions.

(i) The outer-most thinnest surface of the pore-space is determined. This is accomplished by finding those voxels which belong to the pore space but have at least one grain voxel in its 26-

neighborhood. This set of voxel is stored in another matrix; their elements are summed, and divided by the total number of voxels belonging to the porous medium in order to calculate the specific surface area of the system.

(ii) Each of these voxels are taken one by one, eliminated and checked in their 5 voxel x 5 voxel x 5 voxel vicinity if a new three-dimensional object is created because of this elimination. If the outcome is negative then the voxel is designated eligible for elimination.

(iii) All the eligible voxel in the current are iteration are removed from the pore-space data set.

(iv) The resulting thinned three-dimensional data set is stored in a buffer matrix and the original matrix becomes available to the next iteration.

(v) The current buffer matrix is compared for voxel-to-voxel correlation with the previous one. If the outcome is negative then the algorithm continues to the next iteration step.

As a result of following these rules the algorithm stops on its own as it generates the single voxel thin connected skeleton of the pore-space. A flow chart explaining the skeletonization algorithm is given in figure 6. Next, a Euclidean distance transform is done on the complement of the original pore-space matrix, and this three-dimensional map is multiplied voxel by voxel to the binary skeleton matrix. On the skeleton matrix, the voxels are found which has three or more neighbors which belong to the same skeleton. These voxels are designated as the pore centers. The distance-transform values of these voxels correspond to the radius of the pore, which it is the center of. These calculated values of the radii are stored in an array, which translates into the pore size distribution of the reconstructed porous medium. A spherical template based generation of the pores is done based on their respective maximal possible radii. The minimum of the distance-transform map values of all the voxels, belonging to the part of the skeleton that joins two of these pore centers, is the critical radius of that particular throat. The total number of voxels making the current throat is divided by the linear distance between two connected pore centers and is saved as the tortuosity of the corresponding throat.

In order to validate this algorithm, first, a cubic lattice is formed. One sphere is placed at each corner of the cubes. The radii of the spheres are made equal to one half of the sides of the cubes. The arrangement of the spheres is shown in figure 7(a). Now the pore-space not occupied by these spheres is obtained, and passed on to the skeletonization algorithm. The skeleton thus generated is shown in figure 7(b). The algorithm generated pores had all equal radii of the magnitude of 0.83 times the radii of the spheres, which corresponds very well with the analytically calculated value of 0.8284. The skeleton generated in this case also corresponded well with the expected map of it i.e. another cubic lattice.

Results and Discussions

Unconsolidated porous media were reconstructed through the Monte Carlo simulation for five normally distributed particle sizes. Volume rendering of a sample particle packing and pore-space thus created are shown in figures 8(a) and (b), respectively. The particles used had same mean but different variances. The bulk porosity and average number of contacts were calculated through image processing. The effect of particle size distribution width on these computed properties are shown in figures 9, and 10.

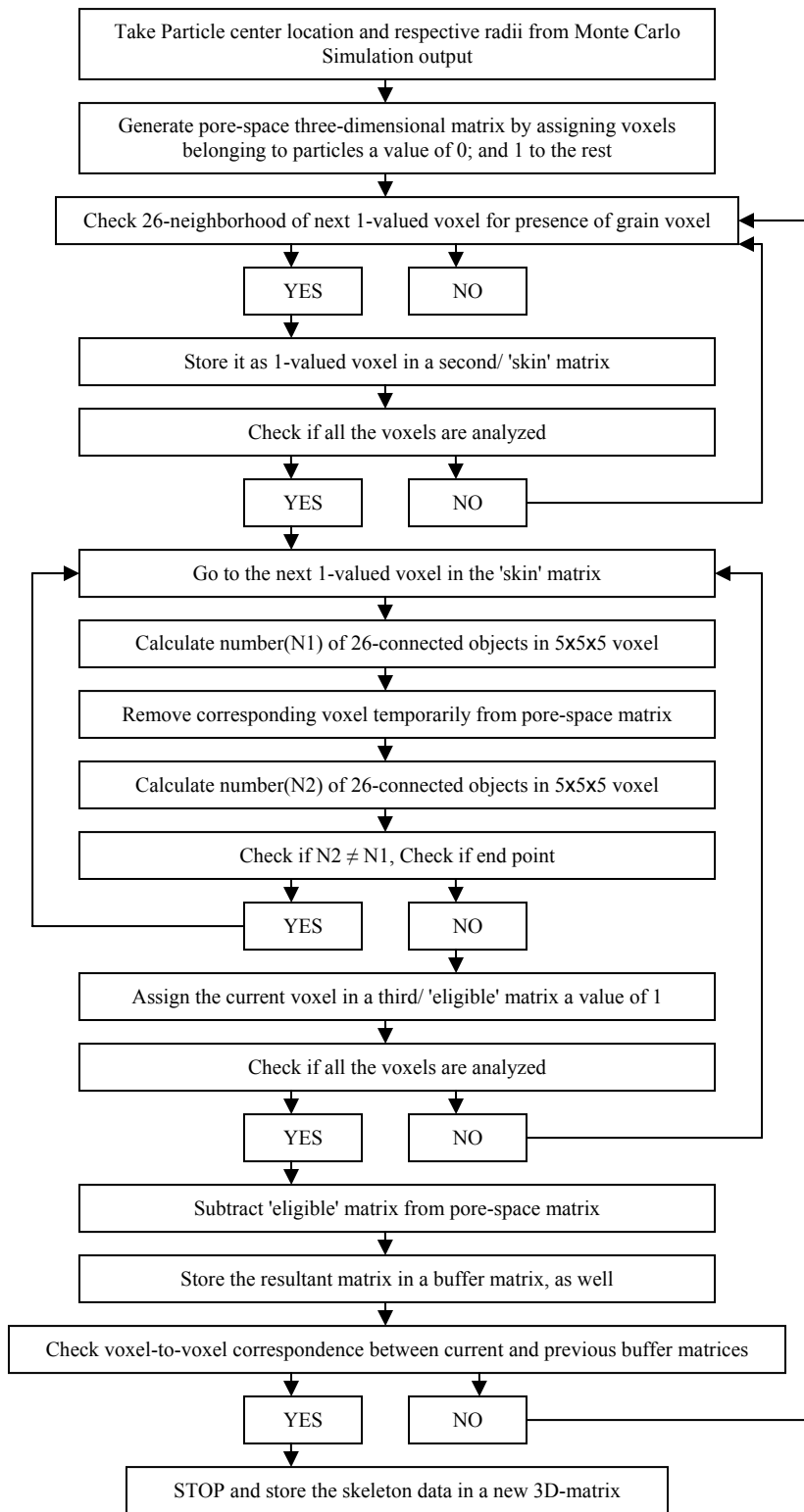


Figure 6: Flow chart of three-dimensional skeletonization algorithm to extract pore network from simulated unconsolidated porous media

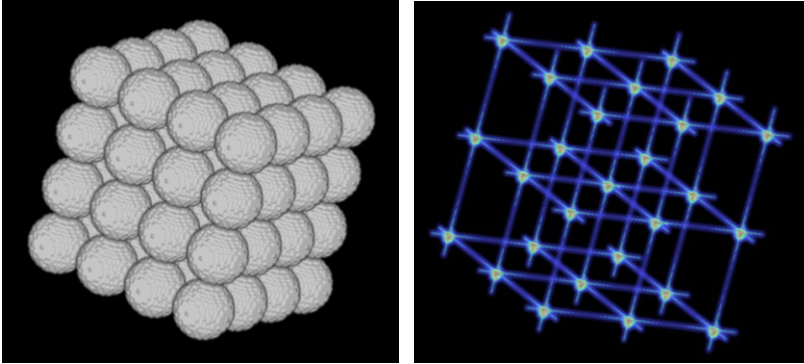


Figure 7: (a) Cubic lattice arrangement of simulated bead pack(on the left); (b) three-dimensional skeleton extracted using current algorithm(on the right)

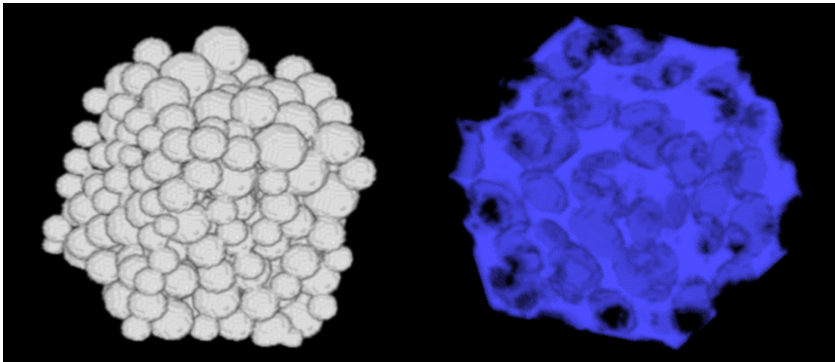


Figure 8: (a) Volume rendering of a Monte Carlo simulated reconstructed porous medium (on the left); (b) Volume rendering of the pore-space (on the right)

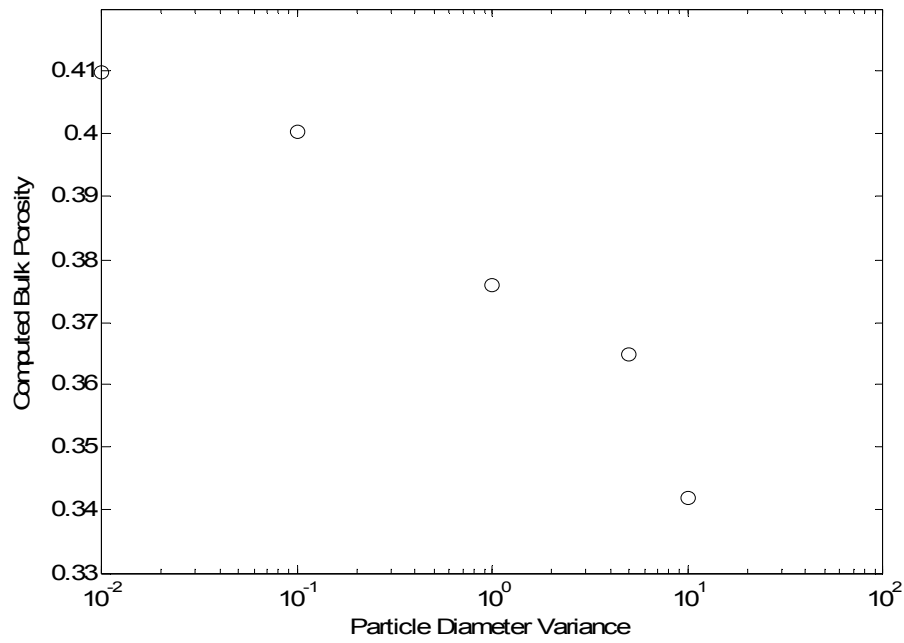


Figure 9: Influence of particle size distribution width on bulk porosity of the reconstructed porous media

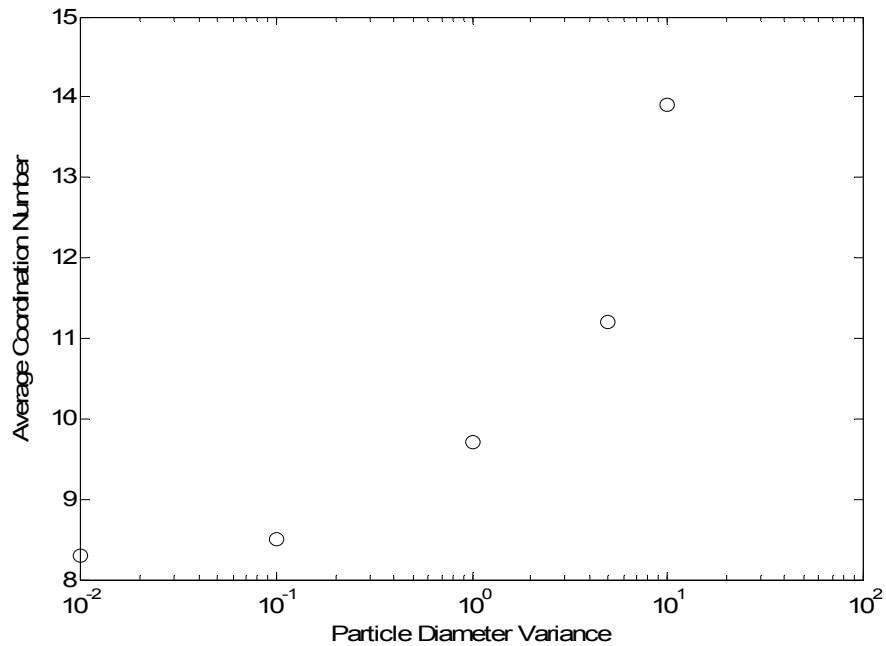


Figure 10: Influence of particle size distribution width on average coordination number of the reconstructed porous media

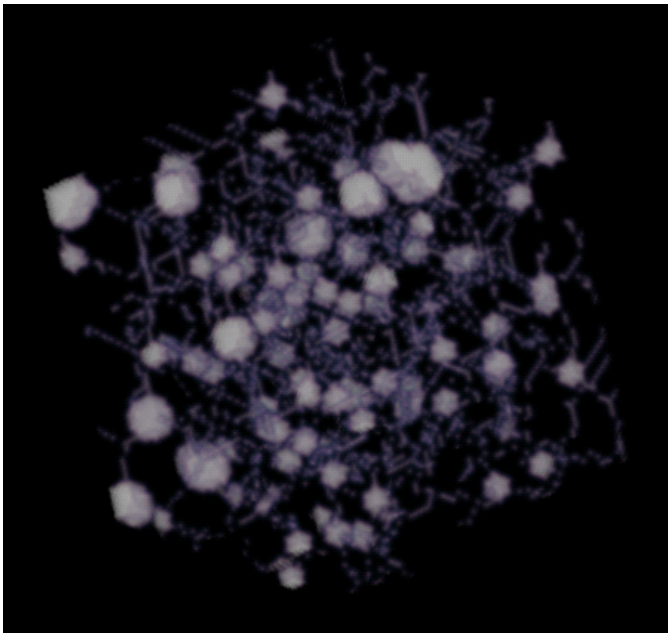


Figure 11: Three-dimensional rendering of a sample extracted pore-network

Size distribution of glass beads of mean diameter 250μ and 500μ are obtained through microscopic image acquisition, automated image analysis (as described in the methods section). These distribution parameters are used as input values in the Monte Carlo simulation algorithm. The pore space data matrices from these reconstructed porous media were then run through the skeletonization algorithm to extract the pore network. Three-dimensional rendering of a sample pore network is shown in figure 11. The pore size distribution, and average tortuosity of the system were computed using the image processing steps described in the methods section. The pore size distributions of those two systems are shown in figures 12, and 13. The average tortuosity of the systems with 250μ , and 500μ mean diameters were 3.97 and 2.04, respectively.

triplicate simulated packs were 0.35, 0.41, and 0.37. A t-test²⁸ comparison ($p < 0.05$) found that the porosity of real glass bead pack and the simulated pack are statistically equivalent. The pore size distribution was extracted from the x-ray microtomography 3D image using the image processing algorithms developed in this work. The extracted pore size distribution is shown in figure 15. A quantitative comparison between the PSDs obtained from simulated pack and the x-ray micrCT image is done by Kolmogorov-Smirnov statistics test. Kolmogorov-Smirnov test statistic is the maximum of absolute differences between two cumulative distribution functions of the distributions being compared²⁹. The value of Kolmogorov-Smirnov statistic in this case is 0.011 which is less than 0.085865, the table value of $w_{1-\alpha}$ quantile with the level of significance (α) as 0.05. Hence, we can accept the null hypothesis i.e. the two PSDs can be considered equivalent.

Although the packing simulation results agree well with the three-dimensional imaging data there are some limitations to this method. The current algorithm can pack particles of spherical shape only. The particles and the container walls are strictly assumed to be hard, so no deformation is allowed. But in real life, many instances can be found where all the constituent particles of a porous material are neither spherical nor perfectly hard. The non-spherical particle situations could be handled by considering geometric constraints related to other shapes while calculating the interaction energy in each iteration of the simulation. The soft boundary condition can be realized by defining a permissible shift window for the container

boundary. But these approaches are not attempted in this work, because the simulation was compared with real glass beads packed in a plastic cuvette both of which had hard boundaries.

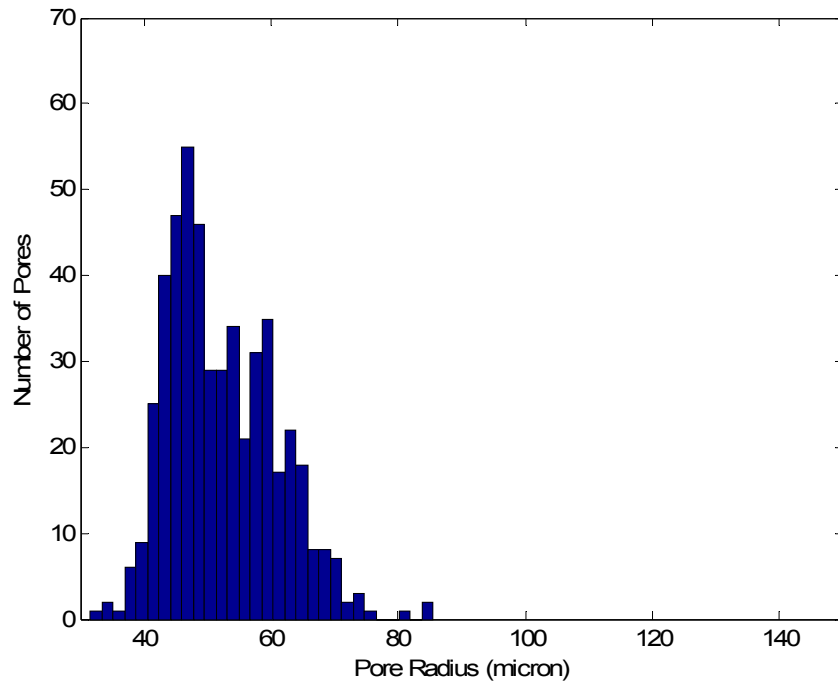


Figure 12: Pore size distribution of 250μ mean diameter particles extracted through skeletonization algorithm applied to simulated packing

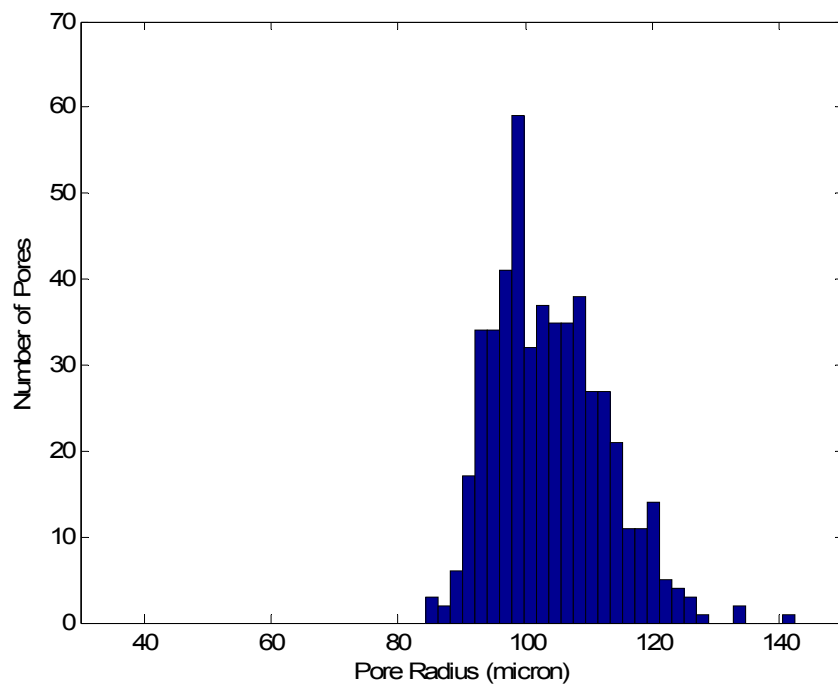


Figure 13: Pore size distribution of 500μ mean diameter particles extracted through skeletonization algorithm applied to simulated packing

The three-dimensional image of a random packing of glass beads of 500 μ diameter as obtained by x-ray microtomography for validation of the packing simulation algorithm is shown in figure 4. The bulk porosity was measured as 0.38. The calculated bulk porosities for the

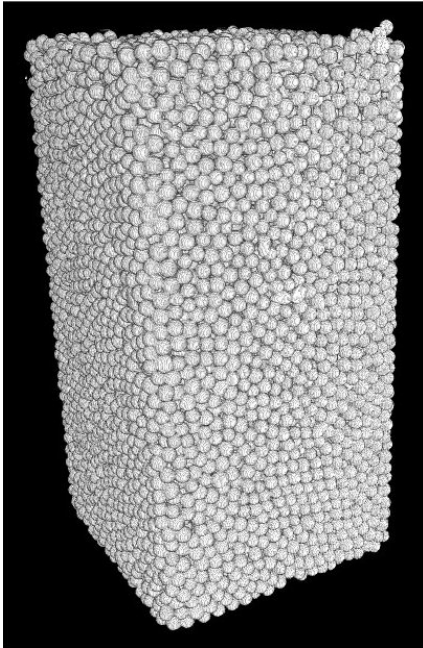


Figure 14: Volume rendering of x-ray microtomographic image of random packing of glass beads

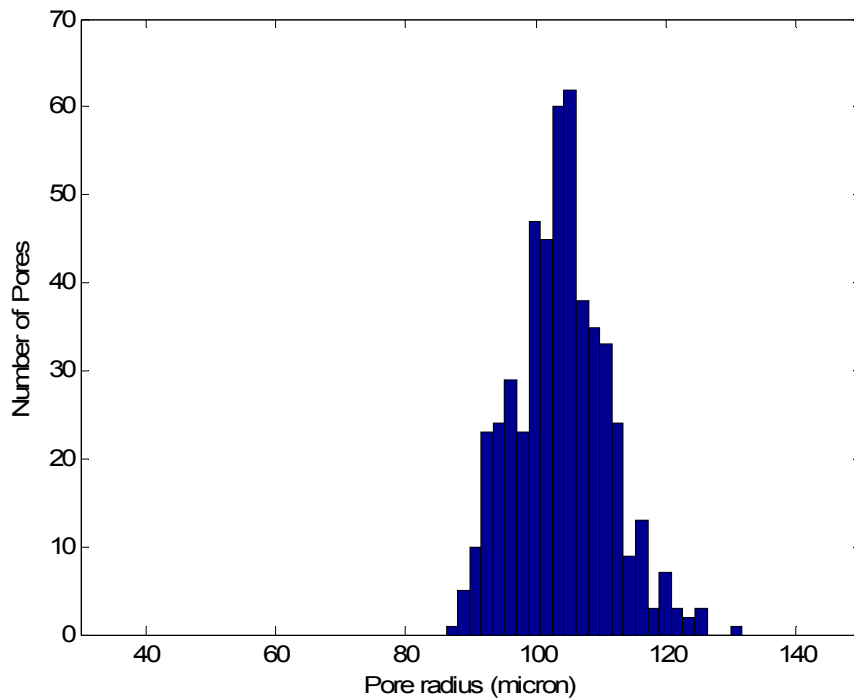


Figure 15: Pore size distribution extracted from x-ray microtomographic image of glass bead pack of 500 μ mean diameter

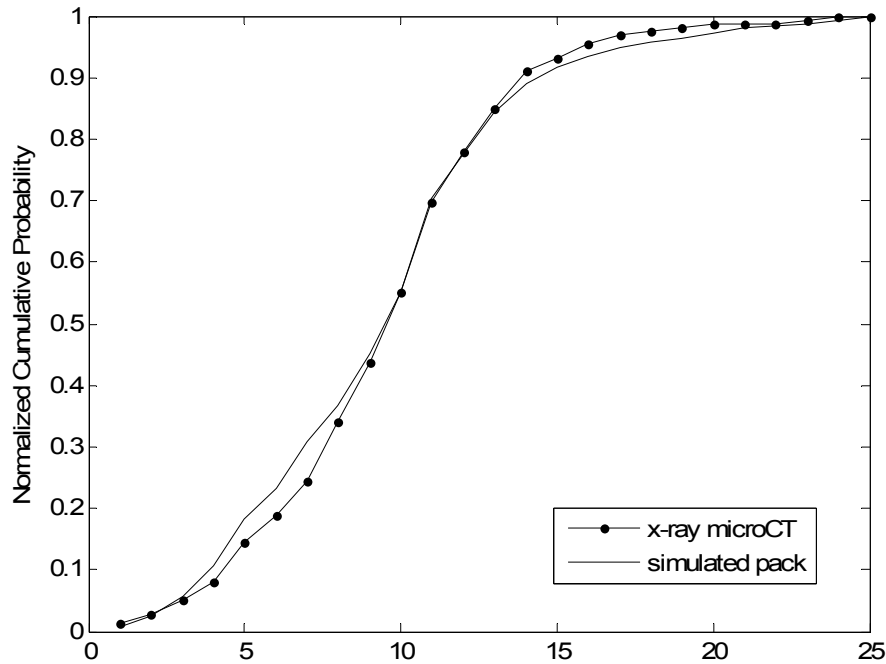


Figure 16: Comparison of normalized cumulative probability distribution from the PSD obtained through x-ray microtomographic image and packing simulation. This is used for the calculation of Kolmogorov-Smirnov statistics.

Conclusions

Porous media is encountered in numerous fields of interest ranging from water resource engineering to process industries. Hence their prediction of transport properties is crucial. Network based modeling of various porous media transport phenomena does not depend on empirically obtained parameters, and accounts for microstructural influence on macroscopic behavior. Hence proper extraction of the pore network becomes instrumental in obtaining realistic prediction. Mapping of the network based on pore-space topology essentially needs the three-dimensional pore-space data set. To obtain this data set through an imaging instrument, the porous media must be created first. Thus only those porous structures which can be created in the laboratory can be utilized in the network based prediction model. But, by means of our current work, a wide range of porous media can be reconstructed, followed by their detailed morphological analysis extracting microstructural parameters relevant to transport modeling. Using this powerful method, virtual experimentation can be done trying out a wide array of possible structures before a very few of them are short-listed for desired transport properties and validated through laboratory experiments. It will not only save time, money and other resources needed in carrying out unnecessary laboratory experiments in the early stages of product development, but also will provide a systematic approach to new porous media based product development.

Acknowledgements

We acknowledge the help of Tom Dufresne of Health Care Research Center, Proctor & Gamble Co., Cincinnati, OH in obtaining three-dimensional x-ray microtomographic image of the random bead pack. We also acknowledge the help of Dr J.D. Miller of University of Utah, Salt Lake City, UT in developing the Monte Carlo simulation.

References

1. Bear J, Buchlin J-M. Modeling and applications of transport phenomena in porous media (1st edition). Dordrecht, The Netherlands: Kluwer Academic Publishers, 1991.
2. Wannan KM, Litchfield JB, Okos MR. Classification of drying models for porous solids. *Drying Technology*. 1993;11:1-17.
3. Whitaker S. Simultaneous heat, mass and momentum transfer in porous media: a theory of drying. *Advances in Heat Transfer*. 1977;13:217-255.
4. Geankoplis CJ. Transport processes and unit operations (3rd edition). New Jersey: Prentice Hall P T R, 1993.
5. Gilliland ER, Sherwood TK. The drying of solids VI: diffusion equations for the period of constant drying rate. *Ind. Eng. Chem*. 1933;25:1134-1141.
6. Masmoudi W, Prat M, Bories S. Drying: percolation theory or continuum approach - some experimental evidences. In: Quiantard M, Todorovic M. *Heat and Mass Transfer in Porous Media*. New York: Elsevier, 1992:817-28.
7. Rogers JA, Kaviany M. Funicular and evaporative-front regimes in convective drying of granular beds. *Int. J. Heat Mass Transfer*. 1992;35:469-478.
8. Laurindo JB, Prat M. Numerical and experimental network study of evaporation in capillary porous media. Phase distributions. *Chem. Eng. Sci*. 1996;51:5171-85.
9. Neimark AV. Multiscale percolation systems. *Sov. Phys. JETP*. 1989;69:786-91.
10. Broadbent SR, Hammersley JM. The mathematics of percolation in networks. *Proc. Cambridge Philosophical Society*. 1957;53:629-35
11. Prat M, Bouleux F. Drying of capillary porous media with stabilized front in two-dimensions. *Phys. Rev. E*. 1999;60:5647-56.
12. Fredrich JT. 3D imaging of porous media using laser scanning confocal microscopy with application to microscale transport processes. *Phys. and Chem. of the Earth*. 1999;24:551-61.
13. Lindquist WB, Venkatarangan A. Investigating 3D geometry of porous media from high resolution images. *Phys. and Chem. of the Earth*. 1999;25:593-99.
14. Oh W, Lindquist WB. Image thresholding by indicator Kriging. *IEEE Transactions on Pattern Analysis and Machine Intelligence*. 1999;21:590-601.
15. Sherwood JD. Packing of spheroids in three-dimensional space by random sequential addition. *J. Phys. A: Math. Gen*. 1997;30:L839-L43.
16. Coelho D, Thovert J-F, Adler PM. Geometrical and transport properties of random packing of spheres and aspherical particles. *Phys. Rev. E*. 1997;55:1959-78.
17. Mort P, Riman RE. Determination of homogeneity scale in ordered and partially-ordered mixtures. *Powder Technology*. 1995;82:94-104.
18. Williams SR, Philipse AP. Random packings of spheres and spherocylinders simulated by mechanical contraction. *Phys. Rev. E*. 2003;67:051301-1-9.
19. Cheng YF, Guo SJ, Lai HY. Dynamic simulation of random packing of spherical particles. *Powder Technology*. 2000;107:123-30.

20. Lam L, Lee S-W. Thinning methodologies – a comprehensive survey. *IEEE transaction on pattern analysis and machine intelligence*. 1992;14:869-85.
21. Siddiqi K, Bouix S. Hamilton-Jacobi skeleton. *Int. J. of Computer Vision*. 2002;48:215-31.
22. Bouix S, Siddiqi K, Tannenbaum. Flux driven automatic centerline extraction. *Medical Image Analysis*. 2005;9:209-21.
23. Ma CM, Sonka M. A fully parallel 3D thinning algorithm and its applications. *Computer Vision and Image Understanding*. 1996;64:420-33.
24. Lee T-C, Kashyap RL, Chu C-N. Building skeleton models via 3-D medial surface/axis thinning algorithms. 1994;56:462-78.
25. Wu QJ, Bourland JD. Three-dimensional skeletonization for computer-assisted treatment planning in radiosurgery. 2000;24:243-51.
26. Hafford KJ, Preston KJ. Three-dimensional skeletonization of elongated solids. *Computer Vision, Graphics, and Image Processing*. 1984;27:78-91.
27. Maddah M, Soltanian-Zadeh H, Afzali-Kusha A, Shahrokni A, Zhang ZG. Three-dimensional analysis of complex branching vessels in confocal microscopy images. *Computerized Medical Imaging and Graphics*. 2005;29:487-98.
28. NIST/SEMATECH e-handbook of statistical methods, <http://www.itl.nist.gov/div898/handbook/>
29. Conover WJ. *Practical Nonparametric Statistics*(1st edition). New York: Wiley, 1998.